doi:10.1006/jmbi.2001.5231 available online at http://www.idealibrary.com on IDEAL® *J. Mol. Biol.* (2002) **315**, 155–170

JMB

A Novel View of Domain Flexibility in *E. coli* Adenylate Kinase Based on Structural Mode-coupling ^{15}N NMR Relaxation

Vitali Tugarinov[1], Yury E. Shapiro[1], Zhichun Liang[2], Jack H. Freed[2]* and Eva Meirovitch[1]*

[1]*Faculty of Life Sciences, Bar-Ilan University, Ramat-Gan 52900, Israel*

[2]*Baker Laboratory of Chemistry and Chemical Biology, Cornell University, Ithaca, NY 14853-1301, USA*

**Corresponding authors*

Adenylate kinase from *Escherichia coli* (AKeco), consisting of a single 23.6 kDa polypeptide chain folded into domains CORE, AMPbd and LID, catalyzes the reaction AMP + ATP → 2ADP. In the ligand-free enzyme the domains AMPbd and LID execute large-amplitude movements controlling substrate binding and product release during catalysis. Domain flexibility is investigated herein with the slowly relaxing local structure (SRLS) model for ^{15}N relaxation. SRLS accounts rigorously for coupling between the global and local N-H motions through a local ordering potential exerted by the protein structure at the N-H bond. The latter reorients with respect to its protein surroundings, which reorient on the slower time scale associated with the global protein tumbling. AKeco diffuses globally with correlation time $\tau_m = 15.1$ ns, while locally two different dynamic cases prevail. The domain CORE features ordering about the equilibrium N-H bond orientation with order parameters, S^2, of 0.8-0.9 and local motional correlation times, τ, mainly between 5-130 ps. This represents a conventional rigid protein structure with rapid small-amplitude N-H fluctuations. The domains AMPbd and LID feature small parallel (Z_M) ordering of $S^2 = 0.2$-0.5 which can be reinterpreted as high perpendicular (Y_M) ordering. M denotes the local ordering/local diffusion frame. Local motion about Z_M is given by $\tau_\parallel \approx 5$ ps and local motion of the effective Z_M axis about Y_M by $\tau_\perp = 6$-11 ns. Z_M is tilted at approximately 20° from the N-H bond. The orientation of the Y_M axis may be considered parallel to the C^α_{i-1}-C^α_i axis. The $\tau_\perp$ mode reflects collective nanosecond peptide-plane motions, interpretable as domain motion. A powerful new model of protein flexibility/domain motion has been established. Conformational exchange (R_{ex}) processes accompany the $\tau_\perp$ mode. The SRLS analysis is compared with the conventional model-free analysis.

Keywords: adenylate kinase; ^{15}N spin relaxation; SRLS; backbone dynamics; intrinsic domain flexibility and domain motion

Introduction

The ability to interpret nuclear spin relaxation properties in terms of microdynamic parameters turned NMR into a powerful method for elucidating protein dynamics.[1,2] The amide ^{15}N spin in proteins is a particularly useful probe, relaxed predominantly by dipolar coupling to the amide proton and ^{15}N chemical shift anisotropy (CSA).[3] The experimental NMR observables are controlled by the global and local dynamic processes experienced by protein N-H bond vectors, which determine the spectral density function, $J(\omega)$. ^{15}N

Present address: V. Tugarinov, Department of Medical Genetics and Microbiology, Faculty of Medicine, University of Toronto, Toronto, Ontario, Canada.

Abbreviations used: AK, adenylate kinase; AKeco, adenylate kinase from *Escherichia coli*; AMPbd, AMP-binding domain; AP_5A, P^1,P^5-di(adenosine-5′)pentaphosphate; CSA, chemical shift anisotropy; HSQC, heteronuclear single-quantum coherence; MF, model-free; NMR, nuclear magnetic resonance; NOE, nuclear Overhauser enhancement; SRLS, slowly relaxing local structure; VALM, very anisotropic local motion.

E-mail addresses of the corresponding authors: eva@nmrsgi1.ls.biu.ac.il; jhf@ccmr.cornell.edu

0022-2836/02/020155–16 $35.00/0

relaxation data in proteins are commonly analyzed with the model-free (MF) approach, where the global and local motions are assumed to be decoupled.[4–6] In a recent study[7] we applied the two-body slowly relaxing local structure (SRLS) approach developed by Freed and co-workers[8,9] to ^{15}N relaxation in proteins. SRLS accounts rigorously for dynamical coupling between the local and global motions, and treats the global diffusion, the local diffusion, the local ordering and the magnetic interactions as tensors that may be tilted relative to one another, providing thereby important information related to protein structure.[10–12] Assessing the accuracy of the MF analysis was possible because the MF spectral density functions constitute asymptotic solutions of the SRLS spectral densities.[8] The SRLS model was parameterized in analogy with the commonly used MF parameterization, and an SRLS-based fitting scheme similar to the MF-based ones was devised. Theoretical simulations and comparative SRLS/MF fitting of experimental data indicated that MF mostly overestimates order parameters, and typically underestimates local motion correlation times, over the parameter range relevant for folded proteins.

Adenylate kinase from *Escherichia coli* (AKeco) is a particularly intriguing case in the context of protein dynamics in general, and the structure-function relationship associated with domain motions in enzymes,[13] in particular. AKeco consists of a single 23.6 kDa polypeptide chain folded into domains CORE, AMPbd and LID. It catalyzes the phosphoryl transfer reaction $Mg^{2+}ATP + AMP \leftrightarrows Mg^{2+}ADP + ADP$.[14] The ribbon diagram of the ''open'' ligand-free form crystal structure[15] is shown in Figure 1(a). CORE is the largest domain. It includes residues 1-29, 60-121 and 160-214 that form a five-stranded parallel β-sheet comprising strands β_1-β_4 and β_9 surrounded by helices α_1 and α_4-α_9. Domain AMPbd includes helices α_2 and α_3 formed by residues 30-59. The LID domain includes residues 122-159, which form a four-stranded antiparallel β-sheet (strands β_5-β_8). Domains AMPbd and LID are displaced significantly upon substrate binding.[15–18] The active site is configured thereby and the ''closed'' structure, illustrated in Figure 1(b) by the ribbon diagram of the complex of AKeco with the two-substrate-mimic inhibitor AP_5A,[19] is obtained. It is assumed that following the reaction the structure ''opens up'' again through reverse movements of AMPbd and LID to recover the original ligand-free enzyme.[15] This mechanism has been inferred based on the crystal structures of ligand-free AK enzymes, and various molecular complexes with nucleoside mono-phosphates, nucleoside tri-phosphates, and inhibitors.[17,20] Time-resolved fluorescence energy transfer studies of fluorescent AKeco derivatives confirmed domain closure in solution upon inhibitor binding.[21,22] These studies also indicated that large-amplitude segmental mobility of AMPbd and LID is in effect in the ligand-free form.[21] Therefore, elucidating the dynamic properties of AKeco bears upon the catalysis-related domain mobility. The time-resolved fluorescence energy transfer experiments focused on a donor-acceptor pair with constituents located in different domains. The ensuing information relates to inter-domain distances and distributions therein. On the other hand, ^{15}N spin relaxation provides unique information on domain flexibility by elucidating the dynamic properties of a large number of N-H bond vectors. Manifestations of nanosecond motions within domains AMPbd and LID of AKeco were detected previously.[23] These results, and the general assessment that in the presence of segmental mobility the global and local N-H motions may not be decoupled, render the SRLS concept of structural and dynamical coupling between motions occurring on arbitrary time scales especially important for the analysis of AKeco dynamics. In this work we have extended the original relaxation data[23] acquired at 14.10 T with ^{15}N T_1, T_2, and ^{15}N-{^1H} NOE data acquired at

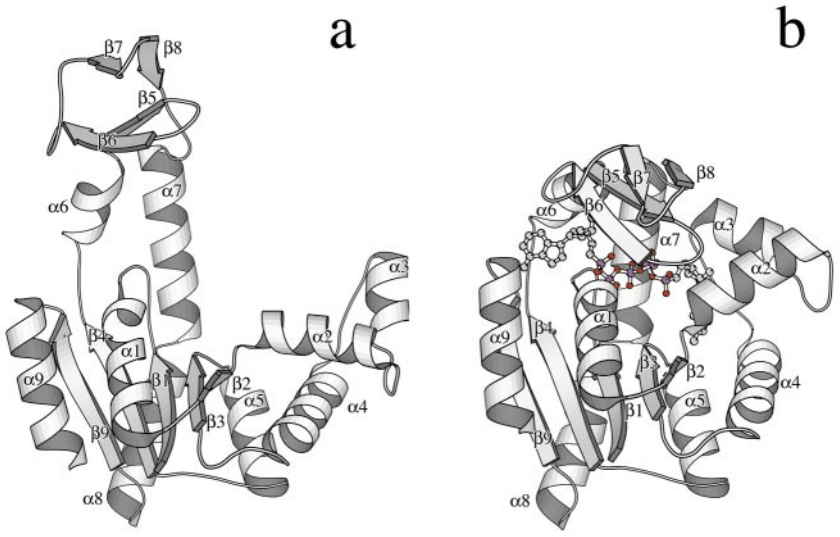

Figure 1. Ribbon diagram of the crystal structures of (a) AKeco and (b) AKeco in complex with the two-substrate-mimic inhibitor AP_5A. The Figure was drawn with the program Molscript[63] using the PDB coordinate files 4ake (complex II) for AKeco and 1ake (complex II) for AKeco*AP_5A.

18.79 *T*, and analyzed the two-field relaxation data using the SRLS approach. It is shown that fundamentally different dynamic models apply to the mobile domains AMPbd/LID, and to domain CORE, which is not engaged in segmental mobility. Domain CORE represents a conventional rigid protein structure with rapid small-amplitude N-H bond vector fluctuations. A new rigorous model of protein flexibility, featuring nanosecond peptide-plane motions, has been established for the domains AMPbd and LID. The nanosecond mode appears to be collective in nature, and can be interpreted as domain motion. Microsecond-millisecond conformational exchange processes akin to segmental mobility accompany it. Implications of nanosecond mode-coupling and multi-site microsecond-millisecond dynamics to the efficiency of common methods for confirming R_{ex} are discussed. The SRLS analysis is compared with the conventional model-free analysis.

Theoretical Background

It was shown in our previous study[7] that the SRLS theory, discussed recently in the context of biomolecular dynamics,[10–12] could be applied to N-H bond vector motions in proteins. The coordinate frames required to describe the SRLS model are depicted in Figure 2(a). The laboratory frame (L) is a space-fixed frame with its *z*-axis along the applied magnetic field. CSA and D are the ^{15}N chemical shift anisotropy and the N-H dipolar magnetic tensor frames, respectively. The dipolar tensor frame has its *z*-axis aligned along the N-H bond (Figure 2(b)). The Euler angles Ω_{LD} and Ω_{LCSA} are the usual stochastic variables of magnetic resonance spin relaxation, modulated by the local motion of the N-H bond vector and the global molecular tumbling. The local diffusion/local ordering frame (M) relates to the local N-H bond vector motions/local ordering potential. The M frame can be tilted relative to the N-H bond (or D frame) by a set of time-independent Euler angles Ω_{MD} (α_{MD}, β_{MD}, γ_{MD}). If we assume the local diffusion/ordering to be axially symmetric only two angles, β_{MD} and γ_{MD}, remain. The global diffusion frame (C) is a molecule-fixed frame determined mainly by the protein shape. The N-H bond vector diffuses in a highly anisotropic environment (due to geometrical and structural/motional restrictions) and experiences local ordering with symmetry axes that may be different from the C frame. We therefore define a local ordering (director) frame C′ that is fixed relative to the C frame. For isotropic global tumbling the distinction between C and C′ frames vanishes (cage frame in Figure 2(a), denoted C below). In summary, the local diffusion of the N-H bond vector and the local ordering induced by the globally tumbling surroundings (cage) are represented by tensors that may be tilted relative to the N-H bond vector (D frame) and the CSA tensor.

The N-H bond vector and the cage (the two ''bodies'') are dynamically coupled by a potential $U(\Omega_{CM})$ that depends on their relative orientation through time-dependent Euler angles $\Omega_{CM}(t)$. The

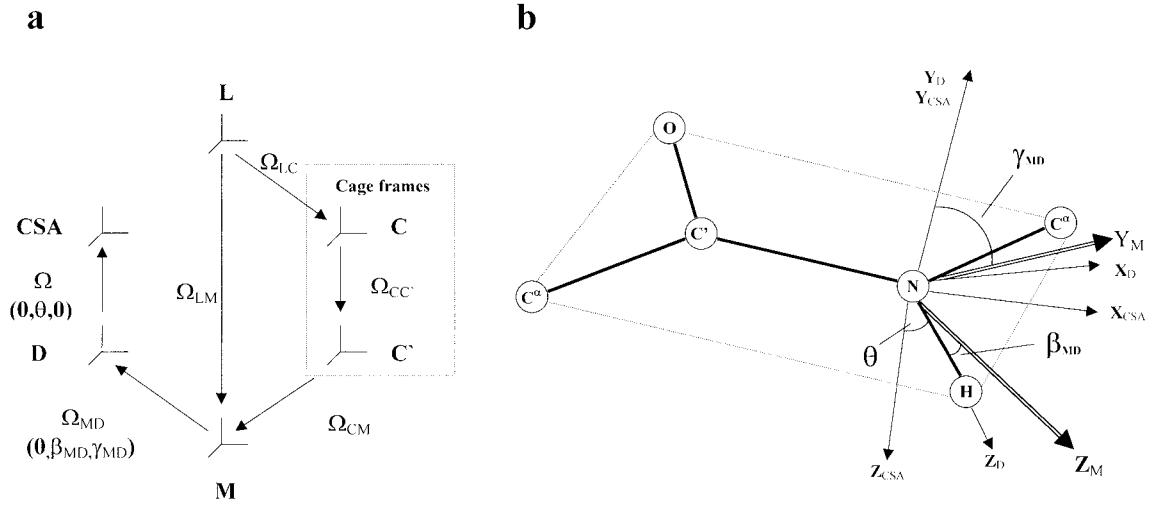

Figure 2. (a) Schematic representation of the coordinate frames used in the calculation of the SRLS spectral density function for the N-H bond vector motions. L, the laboratory frame; C, the global diffusion frame; C′, the local ordering (or local director) frame; M, the local diffusion frame; D, the dipolar ^{15}N-^{1}H tensor frame; CSA, the ^{15}N CSA tensor frame. In the case of isotropic global tumbling the C and C′ frames become the same (cage frame). (b) Definition of the Euler angles associated with the relative orientation of the ^{15}N CSA tensor (X_{CSA}, Y_{CSA}, Z_{CSA}) and dipolar ^{15}N-^{1}H tensor (X_D, Y_D, Z_D) frames. Y_M, Z_M are principal axes of the collinear local diffusion and local ordering tensors. The principal axes X_{CSA}, Y_{CSA}, Z_{CSA} are defined to be aligned with the most shielded (σ_{11}), intermediate (σ_{22}) and least shielded (σ_{33}) components of the ^{15}N shielding tensor, respectively. Y_D and Y_{CSA} are assumed to be perpendicular to the peptide plane.[27] The M → D frame transformation consists of a rotation by an angle β_{MD} about Y_M and a rotation by an angle γ_{MD} about the new orientation of Z_D. The D → CSA transformation consists of a rotation by an angle θ about Y_{DD} (Y_{CSA}).

coupling potential tends to align the N-H bond vector along the principal axes of the ordering frame. In the simplest case of axially symmetric (along Z_M) local ordering it is given by:[10–12]

$$U(\Omega_{CM})/k_BT = -c_{20}D^2_{00}(\Omega_{CM}) \equiv -u(\Omega_{CM}) \quad (1)$$

where k_B is the Boltzmann constant, T the temperature in K, c_{20} the potential strength in units of k_BT, and D^2_{00} the Wigner rotation matrix element. A conventional order parameter can be related to c_{20} as:[10]

$$S_{SRLS} = \langle D^2_{00}[\Omega_{CM}(t)]\rangle \quad (2)$$

The time-dependent part of the spin Hamiltonian for this two-body system is given by:[10]

$$\hat{H} = \sum_{\mu=CSA,D}\sum_{l=0,2}\sum_{m=-l}^{l}\sum_{m'=-l}^{l}\sum_{m''=l}^{l} \times \hat{A}^{(l,m)}_{\mu,L} D^l_{mm'}(\Omega_{LM}) D^l_{m'm''}(\Omega_{MCSA}) F^{(l,m'')*}_{\mu,CSA} \quad (3)$$

where $X^{(l,m)}_{\mu,N}$ stands for the mth component of the lth ($l = 0, 2$) rank irreducible spherical tensor or tensor operator X (where X is either a spin operator $\hat{A}$ or a magnetic tensor F) defined in the N frame, with μ specifying the kind of interaction (^{15}N CSA or ^{15}N-^{1}H dipolar). $D^l_{nn'}(\Omega_{N,N'})$ are Wigner rotation matrix elements which relate the N frame to the N′ frame. The detailed form of $\hat{A}^{(l,m)}_{\mu,L}$ and $F^{(l,m'')}_{\mu,CSA}$ can be found elsewhere.[24]

The dynamic effects of the global and the local diffusion are incorporated into the spectral density through the diffusion operator:[9,10]

$$\hat{\Gamma} = \hat{\Gamma}^{global}(\Omega_{LC}) + \hat{\Gamma}^{local}(\Omega_{LM}) + F^{global}(-\Omega_{CM}) + F^{local}(-\Omega_{CM}) \quad (4)$$

The local motion within the macromolecule (cage) is restricted by the internal orienting potential $U(\Omega_{CM})$ (equation (2)), which couples the global and local motions. The last two terms in equation (4) reflect the contributions to $\hat{\Gamma}$ due to $U(\Omega_{CM})$. F^{global} and F^{local} are functions of the Euler angles Ω_{CM} that transform the M frame into the C frame, which can be further expressed as $(-\Omega_{LC} + \Omega_{LM})$ (Figure 2(a)). This constitutes an effective two-body model for which a Smoluchowski equation representing the rotational diffusion of two interacting rotors is solved.[8,9] The solution features three eigenvalues (correlation times) for the local motion when $S^2 = 0$:

$$(\tau_K)^{-1} = 6R^L_\perp + K^2(R^L_\parallel - R^L_\perp) \quad \text{for } K = 0; 1; 2 \quad (5)$$

Each K value leads to its own spectral density component.[25] Even for $S^2 > 0$ the $j_{K=1}(\omega)$ and $j_{K=2}(\omega)$ components are mainly dominated by local motions, whereas the $j_{K=0}(\omega)$ component represents mixed modes between the global and the local ($R^L_\perp$) motions. The ''measurable'' spectral density is then constructed out of the three $j_K(\omega)$ components by incorporation of the orientation dependent functions that multiply the spin operators in the spin Hamiltonian.[25]

Assuming that the ^{15}N CSA tensor is axially symmetric and collinear with the dipolar N-H tensor ($\theta = 0$ in Figure 1(b)) the spectral density for ^{15}N CSA and ^{15}N-{^{1}H} dipolar relaxation in the coordinate frame of the local motion is given by:[25,26]

$$J(\omega) = Aj_{K=0}(\omega) + Bj_{K=1}(\omega) + Cj_{K=2}(\omega) \quad (6)$$

where

$$A = (1.5\cos^2\beta_{MD} - 0.5)^2, \quad B = 3\sin^2\beta_{MD}\cos^2\beta_{MD},$$

$C = 0.75\sin^4\beta_{MD}$, and β_{MD} is the ''diffusion tilt'' angle between the molecular diffusion axis Z_M and the N-H bond vector. Here, the SRLS parameters featured by $J(\omega)$ include three diffusion rate constants, R^C (global diffusion tensor), $R^L_\perp$ and $R^L_\parallel$ (local diffusion tensor), one potential parameter c_{20}, and the polar angle β_{MD} (diffusion tilt angle) between the M and D frames (Figure 2(b)). Special cases include: (1) isotropic fast local diffusion (local correlation time $\tau_f \equiv \tau_\perp = (6\ R^L_\perp)^{-1} \approx \tau_\parallel = (6\ R^L_\parallel)^{-1}$), implying $\beta_{MD} = 0$; then, $J(\omega) = j_{K=0}(\omega)$, and the NMR relaxation data can be fit with one (c_{20}, if τ_f is negligibly small) or two (c_{20} and τ_f) free parameters, in complete analogy with the original MF formulation;[4,5] (2) very anisotropic slow local motion ($\tau_f \equiv \tau_\parallel \ll \tau_s \equiv \tau_\perp$ and $\tau_f \to 0$), denoted VALM below; then the last two terms in equation (6) are negligibly small compared to $Aj_{K=0}$, provided $\beta_{MD} \neq 54.7^\circ$, and NMR data can be reproduced with three free parameters (c_{20}, τ_s, β_{MD}). The coefficient A in equation 6 is formally analogous to the squared order parameter S^2_f, while S^2_{SRLS} (where S_{SRLS} is calculated using equation (2)) is formally analogous to S^2_s, in the reduced extended MF formula where $\tau_f \to 0$:[6]

$$J(\omega) = S^2_f[S^2_s\tau_m/(1 + \omega^2\tau^2_m) + (1 - S^2_s)\tau'_s/(1 +^2 \tau'^2_s)] \quad (7)$$

S_s and S_f are order parameters associated with the slow and fast local motions, respectively, τ_m is the correlation time of the global motion, and τ'_s is the effective correlation time of the slow local motion. Within the scope of VALM, the fast local motion represents diffusion about Z_M (Figure 2(b)), and the slow local motion represents diffusion of the Z_M axis itself about Y_M. A formal correspondence between the order parameter $S = S_fS_s$ of the extended MF formula and the SRLS order parameter, S, can be established with the relation:

$$S \equiv S_{SRLS}(1.5\cos^2\beta_{MD} - 0.5) \quad (8)$$

A formal analogy is thus established between the reduced extended MF formula"[6] and VALM. If

NMR data at more than one magnetic field are available VALM can be extended by allowing $\tau_f \equiv \tau_\parallel$ to be a free parameter. Then all the $j_K(\omega)$ components contribute to $J(\omega)$ in equation (6). For small β_{MD} angles the SRLS spectral density is formally analogous to the extended MF formula[6] as the term $(1 - S_f^2)\tau_f/(1 + \omega^2\tau_f^2)$, which is now added to the right-hand-side of equation (7), is formally analogous[7] to the second term on the right-hand-side of equation (6).

In principle, the CSA and dipolar magnetic tensors are not collinear (Figure 2(b)). Then, in the local diffusion coordinate frame the dipolar and CSA spectral densities differ. The CSA spectral density can be corrected for non-collinearity[27] with $\Delta J^{csa}(\omega,\theta,\beta_{MD},\gamma_{MD})$ calculated by applying two consecutive rotations: from the M frame to the D frame and from the D frame to the CSA frame.[7] We set $\gamma_{MD} = 90^\circ$ (see below), in which case the diffusion axis of the $\tau_\perp$ mode, Y_M, lies in the peptide plane.

The formal analogy between SRLS and MF spectral densities can be further clarified by giving the actual expression for the SRLS $j_K(\omega)$ functions. The solution of the two-body Smoluchowski equation consists of eigenvalues $1/\tau_i$ and weighing factors c_i, such that:

$$j(\omega) = \sum_i c_i\tau_i/(1 + \omega^2\tau_i^2).$$

The eigenvalues $1/\tau_i$ represent pure or mixed dynamic modes, in accordance with the parameter range considered. The global motion is always given by the smallest eigenvalue, which may be a mixed mode or the pure τ_m mode. The latter case materializes for large time-scale separations between the global and local motions and relatively high ordering. The local motion is generally given by a small number of larger eigenvalues that represent mixed modes. The combined contribution of the dominant modes to $j(\omega)$ can be significantly smaller than 100 %. For large time scale separations and high ordering the relative contribution of the global mode will dominate the spectral density, and the local motion will manifest itself as a large number of mixed modes associated with very large eigenvalues and very small relative weights. The SRLS function $J(\omega)$ is constructed out of the $j_K(\omega)$ components. The $J(\omega)$ from SRLS and from MF have similar general forms and feature the same number of free parameters.[7] In this respect they are ''formally analogous'' but not identical because the MF $J(\omega)$ are not precisely the same dynamic modes and associated weights. Identity is achieved only in the limiting cases where $J(\omega)$ for SRLS yields the MF formulae. We found that the contribution of mixed modes emulates typical experimental errors when $S^2(\text{SRLS}) > 0.9$ and $\tau(\text{SRLS}) < 40$ ps. As indicated by Tugarinov *et al.*,[7] and further demonstrated in this study, the MF limits are not precisely attained over the parameter range relevant to folded proteins. The parameter most sensitive to departures from these limits is τ.

After the spectral density function $J(\omega)$ has been obtained from its fundamental $j_K(\omega)$ components using equation (6), the measurable ^{15}N relaxation quantities ^{15}N T_1, ^{15}N T_2 and ^{15}N-{^{1}H} NOEs are calculated as a function of $J(0)$, $J(\omega_N)$, $J(\omega_H)$, $J(\omega_H + \omega_N)$ and $J(\omega_H - \omega_N)$, using standard expressions for NMR spin relaxation.[3,28]

The theory outlined above has been implemented in a fitting scheme.[7] The SRLS-based dynamic models employed to fit two-field ^{15}N relaxation data of AKeco are summarized in Table 1. In model 1, the local motion is so fast ($\tau \to 0$) that its effect on the spectral density is negligible. This assumption is equivalent in practice to fixing τ at the lowest value for which the SRLS spectral densities could be calculated. In model 2, it is assumed that the internal motion can be approximated as isotropic ($\tau_\perp = \tau_\parallel$). This model is analogous to the original MF formulation. Models 3 and 4 are derived from models 1 and 2, respectively, by addition of the free parameter, R_{ex}, to the transverse relaxation rate expression to account for possible exchange processes on the microsecond to millisecond time-scales. For models $1 - 4$ $\beta_{MD} = 0$, hence $J(\omega) = j_{K=0}(\omega)$ in equation (6), and the correction $\Delta J^{CSA}(\omega)$ depends solely on the angle θ. In model 5 (VALM) the local motion is assumed to be very anisotropic, i.e. $\tau_f \equiv \tau_\parallel \ll \tau_s \equiv \tau_\perp$ and $\tau_f \to 0$. In this case only $\tau_\perp$ (or $j_{K=0}(\omega)$) enters the spectral density. The angle β_{MD} was allowed to vary, affecting $J(\omega)$ through the coefficient A in equation (6). The VALM form of $J(\omega)$ is analogous to the reduced extended MF formula.[6] In model 6 all the terms of equation (6) are considered. As shown previously[7], for small angles β_{MD} the SRLS spectral density $J(\omega)$ becomes formally analogous to the extended MF formula[6]. The restricted local motion is highly anisotropic, with $\tau_\parallel \ll \tau_\perp$.[29] It was found that in this limit $j_{K=1}(\omega)$ and $j_{K=2}(\omega)$ in equation (6) are well approximated by their counterparts for an isotropic local diffusion tensor, with correlation time $1/(6R_\perp^L)$. These approximations were used in models 6 and 8. Models 7 and 8 are derived from models 5 and 6, respectively, by addition of the free parameter R_{ex}.

Results and Discussion

The experimental ^{15}N T_1, T_2 and ^{15}N-{^{1}H} NOE data, acquired at 14.10 and 18.79 T are shown in Figure 3. It can be seen that ^{15}N-{^{1}H} NOE is the most sensitive parameter, with NOE values clearly reduced in the chain regions corresponding to domains AMPbd and LID. T_1 values are lower within AMPbd and within the LID chain segment extending from residue 122 to residue 137. The combined two-field data set was subjected to SRLS analysis, with all the experimental errors leveled to approximately 2.5 %, the χ^2 probability confidence level set at 5 %, and the F-statistic probability confi-

Table 1. SRLS models used to fit experimental AKeco ^{15}N NMR relaxation data acquired at two magnetic fields

No	Parameters[a]	SRLS model description
1	c_{20} (S^2)	Very fast internal motion ($\tau \rightarrow 0$)[b]
2	c_{20} (S^2); τ (τ_f)	Isotropic internal motion
3	c_{20} (S^2); R_{ex}	Model 1 with exchange term
4	c_{20} (S^2); τ (τ_f); R_{ex}	Model 2 with exchange term
5	c_{20} (S_s^2); β_{MD} (S_f^2); $\tau_\perp(\tau_s)$	Very anisotropic internal motion ($\tau_\parallel \rightarrow 0$)[c]
6	c_{20} (S_s^2); β_{MD} (S_f^2); $\tau_\perp(\tau_s)$; $\tau_\parallel(\tau_f)$	Anisotropic internal motion[d]
7	c_{20} (S_s^2); β_{MD} (S_f^2); $\tau_\perp(\tau_s)$; R_{ex}	Model 5 with exchange term
8	c_{20} (S_s^2); β_{MD} (S_f^2); $\tau_\perp(\tau_s)$; $\tau_\parallel(\tau_f)$; R_{ex}	Model 6 with exchange term

[a] Analogous MF parameters are shown in parenthesis.
[b] For model 1 the $\tau \rightarrow 0$ assumption is practically equivalent to fixing τ at the lowest value, for which the SRLS spectral densities can be calculated.
[c] For model 5 the $\tau_\parallel \rightarrow 0$ assumption is equivalent to neglecting the $j_{K=1}(\omega)$ and $j_{K=2}(\omega)$ spectral density components.
[d] For models 6 and 8, where in practice $\tau_\parallel \ll \tau_\perp$, $j_{K=1}(\omega)$ and $j_{K=2}(\omega)$ components calculated for an isotropic local diffusion tensor with correlation time $1/(6R_\perp^L)$ were used in equation (6).

dence level set at 20 %. With these criteria the experimental data of 92.5 % of the residues could be fit using SRLS-based spectral densities.

Global diffusion of AKeco

The determination of the global diffusion tensor R^C was the first step of the analysis. Domains AMPbd and LID of AKeco execute in solution large-amplitude segmental motions.[21,22] On the time scale of the time resolved fluorescence energy transfer experiment this leads to a distribution of conformations.[21,22] On the NMR time scale conformational averaging leads to a well-defined average structure.[23] The global diffusion tensor was determined in a previous study[23] with common methods[30–32] using experimental data acquired at 14.1 *T*. These methods apply to rigid particles while

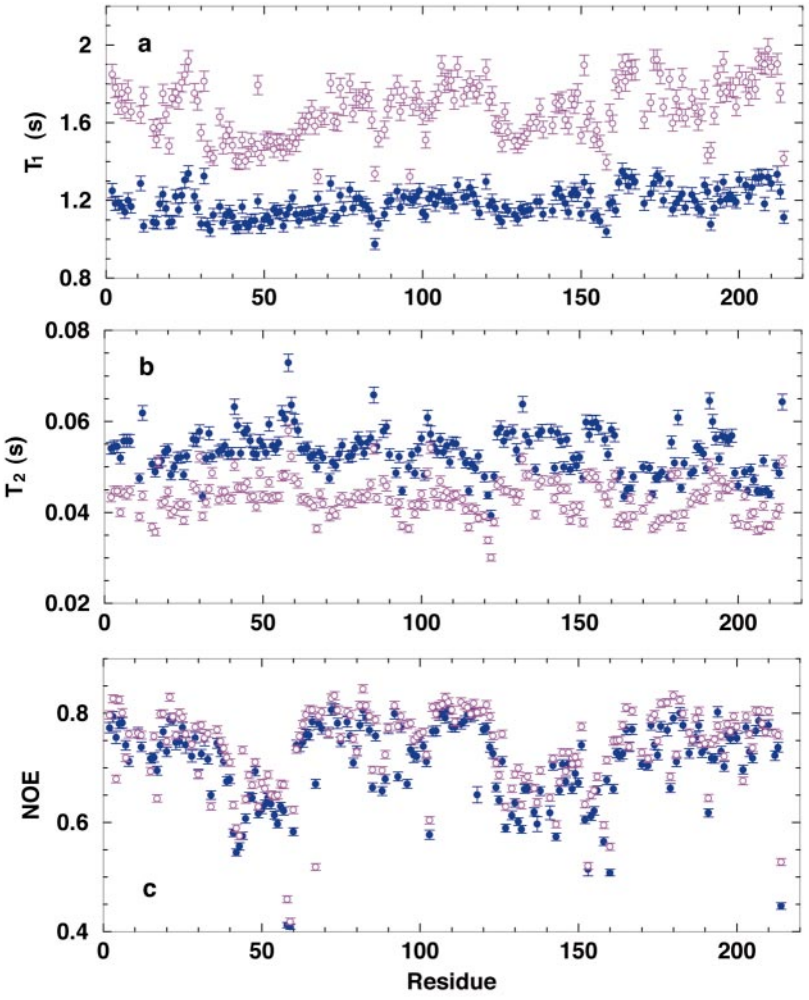

Figure 3. Experimental relaxation parameters (a) ^{15}N T_1, (b) ^{15}N T_2 and (c) ^{15}N-{^{1}H} NOE derived from data acquired at 303 K at 14.10 *T* (filled blue circles) and 18.79 T (opaque magenta circles) as a function of residue number.

AKeco features segmental mobility. As indicated by Shapiro *et al.*,[23] it was necessary to relax to some extent statistical criteria for defining ''rigid spins'', the scatter in the dependence of the apparent local diffusion constant on the N-H orientation was larger than commonly observed, and the diffusion tensor anisotropy obtained, $D_{\|}/D_{\perp} = 1.25$, was significantly smaller than the inertia tensor anisotropy ($D_{\|}/D_{\perp} = 1.49$). Therefore, only general qualitative aspects of the R^{C}-tensor-associated results obtained previously[23] were considered here. These include the conspicuous ''edge'' in the R_2/R_1 profiles within the chain segment Q160-G214 of both AKeco and AKeco*AP_5A, which is very likely to reflect geometric features of the structurally preserved CORE domain (see below discussion of R_{ex} terms associated with this chain segment). On the other hand, the anisotropy factor ($D_{\|}/D_{\perp} = 1.25$) obtained previously[23] is not considered to be an accurate measure of R^{C} tensor anisotropy. Therefore we adopted herein the conservative and physically plausible approach of considering the average AKeco solution structure to be spherically symmetric. The above-mentioned MF calculations yielded an apparent τ_m value of 15.1(±0.5) ns.[23] We used this value in the present study as a τ_m estimate, and scanned the range of 10 to 18 ns in an attempt to refine it with combined data SRLS calculations based on global χ^2 optimization. These calculations confirmed the value $\tau_m = 15.1(\pm 0.5)$ ns. We also found that for $14.5 \leqslant \tau_m \leqslant 15.5$ ns the microdynamic parameters changed slightly, the single-field SRLS results complied with the two-field SRLS results, and the latter reproduced qualitatively the NOE pattern in Figure 3(c). Taken together these data led us to fix τ_m at 15.0 ns in all further calculations.

SRLS dynamics

Microdynamic parameters

The combined two-field data set was subjected to SRLS fitting[7] using the eight SRLS models (Table 1), which can be classified into the simplified models 1-4 and the more general models 5-8. In the first model category it was assumed that R^{L} is in the extreme motional narrowing limit (models 1 and 3) or isotropic (models 2 and 4). The latter simplification is justified when the coupling potential is strong and the time scale separation between R^{L} and R^{C} is large, as in this case $j_{K=0}(\omega)$ is dominated by the global diffusion, and determining R^{L} with reasonable accuracy is difficult. The model 5-8 category includes general cases of weaker coupling potentials and smaller time scale separations, when the tensor R^{L} must be at least axially symmetric. Since $R^{L} \gg R^{C}$ for models 1-4 and $R^{L}_{\perp}$ is on the order of R^{C} for models 5-8, we denote the former parameter range as the ''ps regime'', and the latter parameter range as the ''ns regime''. With a few exceptions the CORE residues were fit with models 2 and 4 and therefore pertain to the ''ps regime''. The AMPbd and LID residues were fit with models 6 and 8 and therefore pertain to the ''ns regime''.

The best-fit microdynamic parameters obtained with the SRLS analysis are depicted in Figures 4 and 5. Squared order parameters, S^2, are clustered into two distinct narrow ranges of 0.78-0.90 in the ps regime and 0.18-0.49 (outlier T15 with $S^2 = 0.04$) in the ns regime. The local motion correlation times $\tau_{\|}$ are shown in Figure 4(b). Note that with models 2 and 4 this parameter represents the presumed isotropic correlation time $\tau \equiv \tau_{\|} \approx \tau_{\perp}$, an assumption validated by the very large time-scale separation between the local and global motions and high order parameters ($\tau_{\|}/\tau_m \leqslant 8.7 \times 10^{-3}$ and $0.78 < S^2 < 0.90$). The τ values display considerable variability, ranging from 5 to 131 ps (six outliers with $155 \leqslant \tau \leqslant 208$ ps). With models 6 and 8 $\tau_{\|}$ represents the parallel component of the local diffusion tensor R^{L}. We found $\tau_{\|}$ to be approximately 5 ps for all the ns regime residues, which practically places $\tau_{\|}$ in the extreme narrowing limit. The slow local motion component $\tau_{\perp}$, associated exclusively with the ns regime, is shown in Figure 4(c). The $\tau_{\perp}$ values span the range of 5.7-11.3 ns (two outliers with $\tau_{\perp} = 5.1$ and 12.8 ns, respectively), with $\tau_{\perp}/\tau_m$ of 0.38-0.75 reflecting the small time scale separation between the global ($\tau_m = 15.1$ ns) and local ($\tau_{\perp}$) motions.

The best-fit values of the coefficient c_{20}, which gauges directly the strength of the coupling potential (equation (1)) associated with the order parameter S_{SRLS} (equation (2)), are shown in Figure 5(a). In the ps regime c_{20} lies within the range of 9.0-20.5 k_BT, whereas in the ns regime c_{20} lies within the range of 2.3-4.7 k_BT (outliers T15 and G214 with c_{20} equal to 1.03 and 5.45 k_BT, respectively). In accordance with the S^2 profile of Figure 4(a), local potentials are strong in the ps regime and, for axial ordering about Z_M, weak in the ns regime. The angle β_{MD} (Figure 5(b)) between the principal axis (Z_M) of the local diffusion (R^{L}) tensor and the N-H bond is of great interest. This unique structural SRLS parameter is not merely an extra variable. As noted above, it is the formal analogue of the extended MF order parameter S_f, in the sense that $1.5\cos^2\beta_{MD} - 0.5 = S_f$. The angle β_{MD} may differ from zero only for models 5-8 associated with the ns regime. The best-fit β_{MD} values (Figure 5(b)) lie between 14.7° and 21.0°. The angle γ_{MD}, which must be specified if the CSA/D tilt angle θ differs from zero, defines the orientation of the ordering axis Y_M. Attempts to vary γ_{MD} in the fitting process led to poorer results than keeping it fixed. This may be associated with β_{MD} and γ_{MD} being correlated because θ is small, and/or because limitations of the experimental data set used do not permit sufficiently accurate and precise determination of six free variables. Further studies will be conducted along these lines after acquiring data at additional magnetic fields. Since γ_{MD} could not be varied freely we tested extreme values. These included $\gamma_{MD} = 0$ and 180°

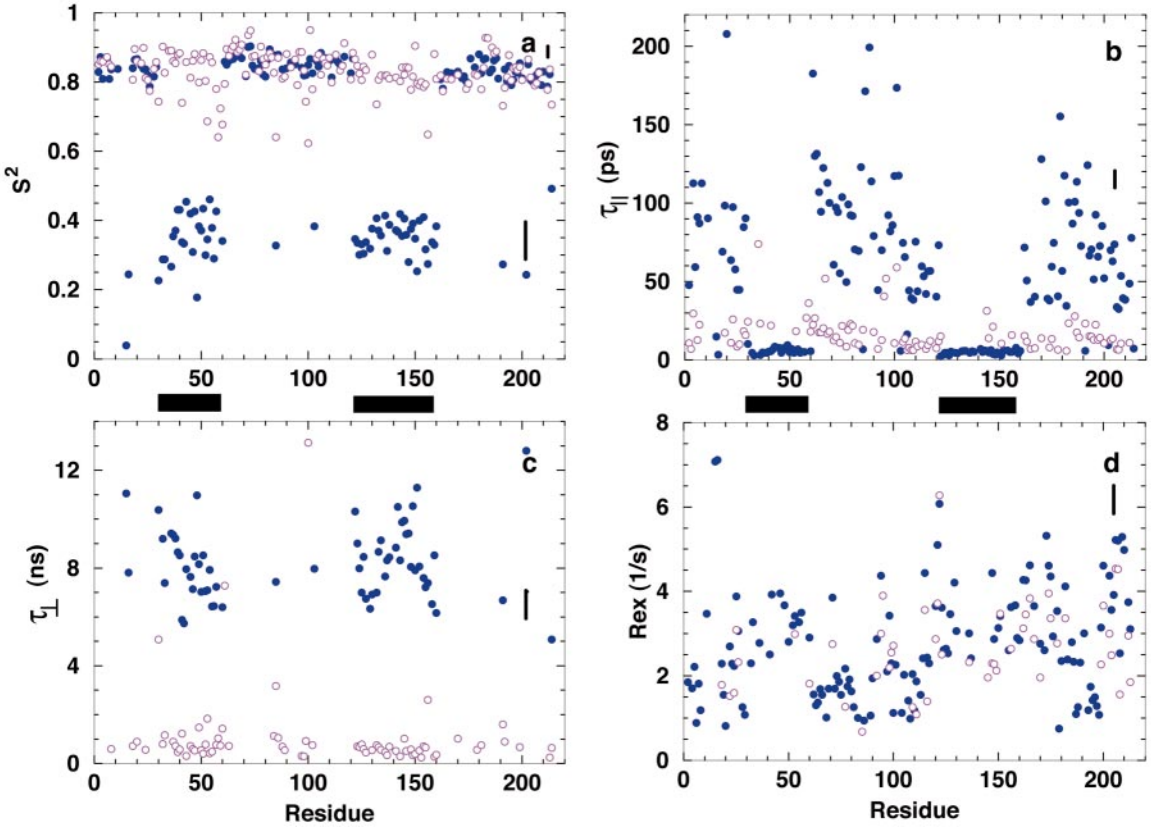

Figure 4. Best fit microdynamic parameters obtained by applying SRLS (filled blue circle) and MF (opaque magenta circles) to the combined data set: (a) squared order parameter, S^2; (b) parallel SRLS local motion correlation time component $\tau_{\|}$ (τ_f in MF); (c) perpendicular SRLS local motion correlation time component $\tau_{\perp}$ (τ_s in MF); and (d) exchange term, 14.10 T R_{ex}, plotted as a function of residue number. For SRLS models 5-8 the squared order parameter, S^2, is calculated as the product of S^2_{SRLS} and $(1.5\cos^2\beta_{MD} - 0.5)^2$, where S_{SRLS} is equivalent to S_s and $(1.5\cos^2\beta_{MD} - 0.5)$ to S_f in the extended MF formula. The SRLS average random errors were as follows: (a) S^2, 1.5 % in the ps regime and 27.8 % in the ns regime, obtained from the Monte Carlo-based random errors in c_{20} using equations (1) and (2); (b) $\tau_{\|}$, 17 (107)% in the ps (ns) regime; (c) $\tau_{\perp}$, 12.1 %; and (d) R_{ex} (14.10 T) up to Q160, 0.63 s^{-1}. Relative MF errors were on the same order of magnitude as the corresponding relative SRLS errors. Average absolute error bars are depicted on the right-hand-side of (a)-(d). The black boxes represent the domains AMPbd and LID. Data were taken from Tables S2 and S3 of Supplementary Material.

(not shown), for which extrema in the γ_{MD}-dependence of the ^{15}N T_1, T_2 and ^{15}N-{^1H} NOE values are encountered, and $\gamma_{MD} = 90^\circ$. The experimental data of a significantly larger number of residues could be fit with $\gamma_{MD} = 90^\circ$. The latter value places Y_M within the peptide plane, possibly parallel to the C^{α}_{i-1}-C^{α}_i axis[33] (or eventually the N_i-C^{α}_i bond). Hence we assigned the value of 90° to γ_{MD}. For axial Z_M ordering, $\gamma_{MD} = 90^\circ$ and $\beta_{MD} \approx 20^\circ$ the Z_M axis assumes an out-of-plane orientation. We examine below qualitatively asymmetric ordering. A quantitative treatment thereof is required to determine the M frame accurately.

Physical models

The ps model features S^2 and τ as free SRLS variables. It represents a rigid protein structure with rapid small amplitude fluctuations about the equilibrium N-H bond orientation. This corresponds to high S^2 and low τ. The ns model features S^2, $\tau_{\perp}$, $\tau_{\|}$ and β_{MD} as free SRLS variables. The time scales of $\tau_{\|}$ and $\tau_{\perp}$ differ significantly, representing within a good approximation individual motions restricted about Z_M and Y_M, respectively. Asymmetric Y_M ordering with Z_M preferred over X_M, and the approximate decoupling of the $\tau_{\|}$ and $\tau_{\perp}$ modes, is featured by a previously developed SRLS spectral density[29] validated in the mode-decoupled limit, which is formally analogous to the extended MF formula.[6] Hence the rigorous approach is to define the main ordering axis as Y_M and use the potential function:

$$U(\Omega_{CM})/k_BT = -3/2c_{20}^{aniso}\cos^2\beta_{MD} - \sqrt{6}/2c_{22}^{aniso}\sin^2\beta_{MD}\cos(2\gamma_{MD})^{35}$$

which reduces to $-(3/2\ c_{20}^{aniso} + \sqrt{6}/2\ c_{22}^{aniso})\cos^2\beta_{MD} + \sqrt{6}/2c_{22}^{aniso}$ for $\gamma_{MD} = 90^\circ$. In principle potential coefficients can be recalculated for varying principal ordering axes.[35] However, we used the simplified one-term potential $U(\Omega_{CM})/k_BT = -3/2\ c_{20}\cos^2\beta_{MD}$ (equation (1)) for axial parallel

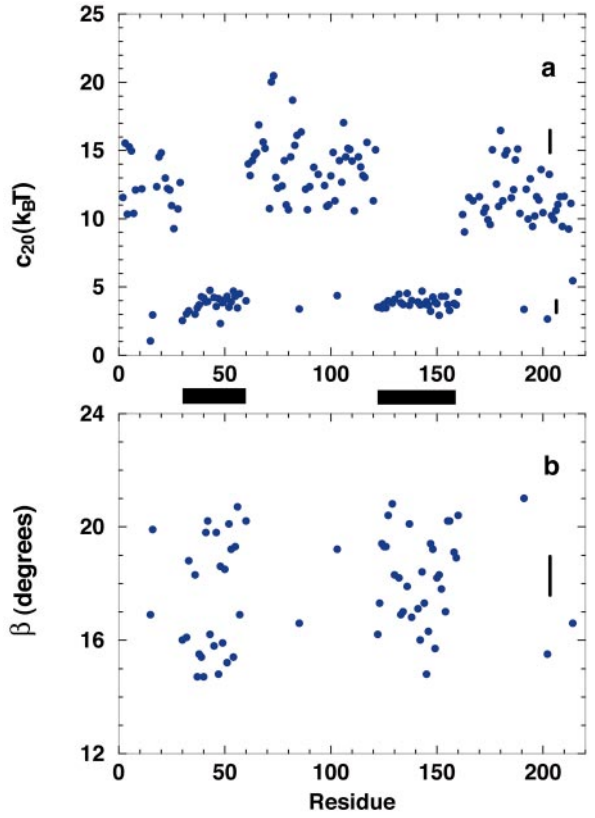

Figure 5. Fig. 5. (a) Best fit microdynamic parameters obtained by applying SRLS to the combined data set: (a) the coupling potential coefficient c_{20} (equation (1)) corresponding to S_{SRLS} (equation (2)), and (b) the tilt angle β_{MD} between the collinear local diffusion and ordering axes, and the principal axis of the magnetic dipolar tensor, plotted as a function of residue number. The average random errors were as follows: (a) c_{20}, 12.6 % in the ps regime and 17.3 % in the ns regime; and (b) β_{MD}, 1.4°. Average absolute error bars are depicted on the right-hand-side of (a) and (b). The black boxes represent the domains AMPbd and LID. Data were taken from Table S2 of Supplementary Material.

(Z_M) ordering (which based on the geometry outlined in Figure 2 is expected to be very insensitive to deviations from axial symmetry). Therefore at the moment we only recall that low parallel ordering is equivalent to high perpendicular ordering,[35] and interpret qualitatively the low S^2 values obtained as high restrictions about Y_M and Z_M. Extension of our current SRLS/NMR implementation to an asymmetric local potential is underway. Determining both c_{20}^{aniso} and c_{22}^{aniso} is expected to provide important new insight into local structure and dynamics in proteins. We mention in this context the work of Brüschweiler *et al.*[33,36,37] on S^2 interpretation in terms of fast asymmetric N-H fluctuations. It was found that the C^{α}_{i-1}-C^{α}_{i} axis is associated with the largest fluctuation amplitudes.[33] Setting $\gamma_{MD} = 90°$ in our SRLS calculations complies with Y_M nearly parallel to C^{α}_{i-1}-C^{α}_{i}, implying ns ($\tau_{\perp}$) motions about this axis. It may be useful to combine the two approaches in the future.

Parameter magnitudes can now be rationalized. The $\tau_{\parallel}$ mode is in the extreme-motional-narrowing limit to establish an equilibrium orientation about the tilted Z_M axis. The tilt angle β_{MD} is on the order of 20°, complying with the approximate perpendicular orientation of the N-H bond and the C^{α}_{i-1}-C^{α}_{i} axis[33] (as well as the angle H-N-C^{α} of 113°).[34] $\gamma_{MD} \approx 90°$ is compatible with the diffusion axis Y_M of the $\tau_{\perp}$ mode lying along the C^{α}_{i-1}-C^{α}_{i} axis. This concurs to $\tau_{\perp}$ representing peptide plane motion, as both the diffusion axis, C^{α}_{i-1}-C^{α}_{i}, and the diffusing axis, Z_M, are close to the peptide plane. Since all the parameters are highly clustered this mode is apparently collective, hence interpretable as domain motion. Thus, the various parameters must be close to the noted values for the ns model to be meaningful. On the other hand, the inherent sensitivity,[7] and the accuracy of the SRLS analysis, also render site-specific research meaningful. Accounting for asymmetric ordering will provide further options in this respect.

It is concluded that bimodal parameter clustering reflects the specific nature of N-H bond dynamics. The ps and ns models apply to different parameter ranges because they differ. Clustering within each range is implied by the physical nature of the respective model. There is nothing in-between, since it is difficult to conceive of local motions besides fast N-H fluctuations and slow peptide plane motions experienced by a backbone-attached N-H bond restricted to the peptide plane. Under different physical circumstances, such as a spin probe attached to a protein *via* a long flexible linker,[38] continuous parameter values are physically possible, and were indeed observed. The original MF and extended MF models are simplified versions of the SRLS ps regime and ns regime models, respectively, so the results of MF fitting should also feature two parameter clusters. However, the MF microdynamic parameters are inaccurate.[7] The MF S^2 profile appears to be continuous (Figure 4(a)) because MF over-estimates S^2 to a much larger extent in the ns regime than in the ps regime. On the other hand MF τ_f and τ_s differ to a much larger extent. Consequently they also feature parameter clustering (Figure 4(b) and (c)).

It is appropriate to examine the exceptional CORE residues associated with ns regime parameters. Within the ps CORE region the ns outliers include residues T15, Q16, T60, G85, R88, V103, Q160, T191, V202 and G214. Residues T15, Q16 and G122 are unique in being associated with $6.1 \leqslant R_{ex} \leqslant 7.1\ s^{-1}$ (Figure 4(d)). Residue T15, associated with an exceptionally low order parameter (Figure 4(a)), is hinge 1.[15] Residues T15 and Q16 belong to the P-loop,[19] indicating flexibility of this important nucleotide binding motif. Q60 and Q160 are adjacent to the C-terminal residues of the mobile domains. V103 is the C-terminal residue of loop α_5/β_4, T191 belongs to loop α_8/β_9, and R88

may bind to the α-phosphate of AMP.[19] The fitting scheme led originally to several rigid outliers fitted with models 2 or 4 within the largely flexible AMPbd/LID domains. This was difficult to rationalize on physical grounds. The microdynamic parameters associated with these outliers were examined carefully. The respective τ values turned out to exceed consistently the average τ value of true ps minima. (Figure 4(b)). This is an indication that the fitting program may have converged to non-physical minima, as the ps model is only justified when τ/τ_m is very small. As indicated above, the ps and ns regime models are the only options for N-H bond dynamics and the associated parameters are clustered into two distinct regions. Hence minima located in the connecting parameter region do not correspond to a physical model. The ns fitting scenario tests the simpler models 1-4 first using ps regime starting points, and the more complex models 5-8 next using ns regime starting points. Hence it is possible that in the first trial non-physical minima located outside of, but adjacent to, the ps parameter cluster are reached. We found that all of the AMPbd and LID outliers converged initially to such minima. Convergence to the genuine ns minima was achieved by using exclusively ns regime starting points. Non-physical minima can be diagnosed based on unusually high τ values.

Further implications and data analysis issues

The dynamic state of loops α_4/β_3 and α_5/β_4 can be related to the ''energetic counter-balancing of substrate binding'' concept set forth by Müller *et al*.[15] Based on crystallographic *B*-factors these authors found that in the AKeco-AP_5A complex the active site is rigid, whereas loops α_4/β_3 and α_5/β_4 are flexible. Conversely, in the ligand-free enzyme the active site is flexible, whereas loops α_4/β_3 and α_5/β_4 are rigid. The ''solidification'' of loops α_4/β_3 and α_5/β_4 upon substrate release is hypothesized to serve as a ''counterweight'' balancing the substrate binding energy. This hypothesis was confirmed by a previous solution ^{15}N NMR relaxation study.[23] The present SRLS analysis indicates that loops α_4/β_3 and α_5/β_4 (except for residue V103) are rigid in AKeco.

The results presented thus far were based on the analysis of the two-field six-point data set. The single-field three-point data sets were also analyzed separately. The three-point SRLS fitting was found to be satisfactory in the ps regime but less robust in the ns regime. For example, a larger number of ns residues were mis-assigned as apparent ps residues with three-point data than with six-point data. However, these mis-fits can be corrected, as outlined above.

Conformational exchange

The 14.10 *T* R_{ex} contributions determined by SRLS are shown in Figure 4(d). It is highly desirable to confirm experimentally R_{ex} data determined as best-fit parameters. This is typically accomplished based on $R_{1\rho}$ or CPMG experiments,[39] and/or on measurements of ^{15}N CSA-^{15}N-^{1}H dipolar cross-correlation rates η_{xy}.[40]

We carried out $R_{1\rho}$ experiments with $\omega_1 = 2.5$ kHz at 14.10 *T* on AKeco. If the exchange process is in the motional narrowing limit $\omega_1 = 2.5$ kHz is expected to obliterate R_{ex}, and the difference $R_2 - R_{1\rho}$ is expected to match the R_{ex} value obtained as best-fit parameter (see Millet *et al*.,[39] and papers cited therein). Only 32 % of the best-fit SRLS R_{ex} values of AKeco were confirmed in this manner. To ascertain that experiment and analysis are appropriate we subjected the complex of perdeuterated ^{15}N-AKeco with the inhibitor AP_5A (D-AKC) (work in progress) to the same treatment as AKeco. With D-AKC the differences $R_2 - R_{1\rho}$ confirmed nearly 70 % of the SRLS R_{ex} data. We assign this to differences in the conformational exchange characteristics of the two protein systems. AKC is a conventional rigid molecular complex apparently experiencing commonly assumed fast two-site conformational exchange. AKeco prevails in solution as an ensemble of conformations in thermodynamic equilibrium,[21–23] most likely experiencing arbitrary-time-scale multi-site exchange. Millet *et al*.[39] investigated two-unequal-site exchange with relaxation-compensated CPMG methods. The decay rate of the apparent exchange contribution, $R_2(1/\tau_{cp})$, was found to be reduced in the slow and intermediate time regimes relative to the exchange-narrowed time regime. In some cases R_{ex} was not cancelled with the highest pulsing rate attainable, which is analogous to $\omega_1 = 2.5$ kHz in our $T_{1\rho}$ experiments. With arbitrary-time-scale multi-site exchange the decay of the apparent exchange contribution may be even slower, eventually undetectable experimentally. Also, the effective line broadening may be very sensitive to temperature instabilities during long accumulation periods. Therefore with AKeco lack of compliance of the $R_2 - R_{1\rho}$ ($\omega_1 = 2.5$ kHz) differences with the best-fit SRLS R_{ex} data does not necessarily prove the latter are not genuine. Also, under these circumstances the common quadratic-field-dependence test may not be useful, as for slow and intermediate exchange $R_2(1/\tau_{cp})$, hence $R_{1\rho}(\omega_1)$, exhibits non-quadratic field-dependence.[39]

^{15}N CSA-^{15}N-^{1}H dipolar cross-correlation rates (η_{xy}) can be used in concert with R_2 data to confirm best-fit R_{ex} terms. The underlying concept is the model-independent approach,[40] which assumes that the local motions can be described as independent small, equal amplitude restricted rotations about three mutually orthogonal axes, in which case $J(\omega)$[cross-correlation] = $(1.5\cos^2\theta - 0.5)J(\omega)$[dipolar].[41] The method[40] consists of plotting η_{xy} *versus* R_2. Points that digress from the diagonal toward higher R_2 values imply association with R_{ex}. In a previous study based on MF analysis and 14.10 *T* data we found that practically all the best-fit R_{ex} terms of AKC, but very few

best-fit R_{ex} terms of AKeco, are confirmed in this manner.[23] The same picture is obtained with SRLS-determined R_{ex} terms. The model-independent assumptions appear to be justified for the outstandingly rigid molecular complex AKC, but unjustified for AKeco, where the local motions cannot possibly be described as outlined above. Indeed, preliminary SRLS studies of η_{xy} indicate that deriving $J(\omega)$[cross-correlation] from $J(\omega)$[dipolar] as outlined above is highly inappropriate for ns residues. Hence the η_{xy}-based method is not successful with AKeco.

Since experimental confirmation of R_{ex} turned out to be problematic we resorted to semi-quantitative considerations. The experimental R_2 data, given by $R_2(\mathrm{SRLS}) + R_{ex}$, do not distinguish between the ns domains AMPbd/LID and the ps domain CORE (Figure 3(b)). This indicates that R_{ex} terms are compensating for lower R_2(SRLS) in the ns regime. It can be seen (Figure 4(d)) that the R_{ex} contributions are distributed non-uniformly over the polypeptide chain. As indicated in the Global diffusion of AKeco section, above, the global diffusion anisotropy was accounted for explicitly in a previous study based on data acquired at 14.1 *T*.[23] The only firm manifestation of global diffusion anisotropy is the conspicuous ''edge'' in the R_2/R_1 profile within the chain segment Q160-G214. A similar ''edge'' within this chain segment is visible in the R_{ex} profile (Figure 4d), indicating that these R_{ex} data are likely to have absorbed geometric effects associated with R^C anisotropy. Therefore R_{ex} terms within the chain segment Q160-G214 are disregarded in the present discussion of genuine conformational exchange contributions. The possibility that R_{ex} in the remaining part of the chain represents fudge factors associated with the SRLS fitting was excluded by back-calculated 14.10 *T* R_2(SRLS) data using typical ns and ps regime parameters. We found with simulations that $R_2(\mathrm{SRLS})(\mathrm{ps}) - R_2(\mathrm{SRLS})(\mathrm{ns}) \approx 2\ \mathrm{s}^{-1}$, whereas Figure 4(d) indicates that on average $R_{ex}(\mathrm{ns}) - R_{ex}(\mathrm{ps}) \approx 2\ \mathrm{s}^{-1}$. We conclude that within AMPbd/LID and the CORE region below Q160 the best-fit R_{ex} terms represent genuine conformational exchange. The larger contributions with the mobile domains are actually implied by the very nature of segmental mobility.

Model-free *versus* SRLS

Parameter comparison

The mode-decoupled MF formulae are asymptotic solutions of the mode-coupled SRLS spectral densities. We found previously[7] that in general SRLS generates a significantly more accurate and discriminating dynamic picture than MF. It is of interest to examine the implications of these findings to AKeco dynamics. To this end MF analysis was carried out and compared with SRLS analysis. Using the same statistical criteria the experimental data of 19 % of the residues were not fit with MF, as compared to the experimental data of 7.5 % of the residues not fit with SRLS.

The MF and SRLS model-category selection (but not the individual model selection) patterns were found to be generally similar. The best-fit parameters obtained with MF are shown in Figure 4(a)-(c) together with the corresponding SRLS parameters. The S^2 MF data (Figure 4(a)) lie mainly within the range of 0.8 to 0.9. The highest value is 0.95 and the lowest 0.6, with only six S^2 values below 0.7. In the ps regime MF S^2 is mostly higher than SRLS S^2, in excess of the experimental error. In some cases they are practically the same. In the ns regime MF S^2 overestimates SRLS S^2 on average by 131 %. With MF domain AMPbd is singled out by only three (five) residues with S^2 below 0.7 (0.75), whereas domain LID is singled out by only one residue (two residues) with S^2 below 0.7 (0.75). Clearly S^2 MF distinguishes very poorly between domains AMPbd/LID and CORE, contrary to the raw NOE data (Figure 3(c)). The limited discriminating power of MF is illustrated in Figure 6(a), where the ribbon diagram of the AKeco crystal structure is color-coded according to MF S^2. The high discriminating power of SRLS is illustrated in Figure 6(b). The MF τ_f and τ_s profiles do single out AMPbd and LID qualitatively (Figure 4(b) and (c)). This is illustrated in Figure 7(a), where the ribbon diagram of the AKeco crystal structure is color-coded according to MF τ_s. Thus, for AKeco MF τ_s is more useful than MF S^2 in diagnosing ns local motions associated with low NOEs. Actually it emulates SRLS in this respect, as indicated by comparison with Figure 7(b), where we show the SRLS counterpart of Figure 7(a). The quantitative differences are, however, substantial (Figure 4(c)), with MF τ_s (yellow in Figure 7(a)) under-estimating SRLS $\tau_\perp$ (red in Figure 7(b)) on average by a factor of 11. The SRLS $\tau_\perp$ values and the global correlation time τ_m are comparable in magnitude, with the spread in $\tau_\perp$ being only 33 % about the mean, supporting the notion of cooperative flexibility. On the other hand MF τ_s is on average tenfold faster than τ_m, and the spread in τ_s is ~200 %.

The $\tau_\parallel$ (τ_f) data are presented in Figure 4(b). In the ps regime the MF τ_f value ranges between 5 and 50 ps, and its SRLS counterpart ranges mostly between 5 and 131 ps. Analysis of corresponding pairs indicated that MF underestimates local motion correlation times by factors of 3-6. These large factors may impact significantly on the concept of rigid residues and τ_m determination.[30] It is noteworthy in this context that theoretical S^2 values of rigid residues, calculated recently with the mode-coupling diffusion theory,[42] were lower than S^2 values derived from NMR data obtained with the vnd/NK-2 homeodomain from *Drosophila melanogaster*, indicating that this protein may not feature rigid residues.

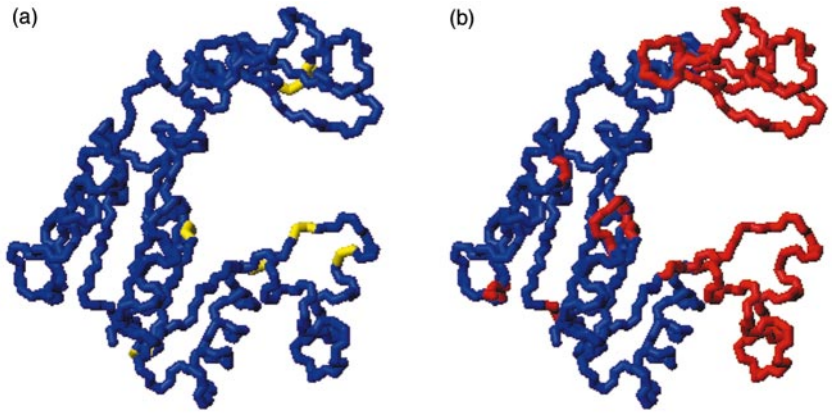

Figure 6. Ribbon diagrams of the crystal structure of AKeco color-coded according to MF S^2 values (a) and SRLS S^2 values (b). The Figure was drawn with the program Molscript[63] using the PDB coordinate file 4ake, and color-coded using the program MOLMOL[64]. Residues with $S^2 \geqslant 0.7$ are colored blue. Residues with $0.6 < S^2 < 0.7$ are colored yellow and residues with $S^2 \leqslant 0.55$ are colored red. The color-coding is in accordance with Figure 4(a).

Analysis of the MF S^2profile

As indicated above, the MF S^2 profile (Figure 4(a)) does not reproduce the NOE profile (Figure 3(c)). This is contrary to the common observation. Within the scope of pinpointing the underlying reasons NOEs were measured at 11.7 *T* and added to the six-point 14.10/18.8 *T* data set. The MF S^2 profile changed marginally. Practically identical results were obtained with different implementations of the model-free formalism.[32,43] The MF S^2 profile was also found to be largely invariant to changes in random NOE errors between 1.5-2.5 %.

As shown in the Conformational exchange section above, the R_{ex} terms within AMPbd and LID are most probably genuine. Yet, MF fails to identify most of these terms, in disagreement with the raw R_2 data, and contrary to the very nature of segmental mobility. There is only one MF R_{ex} term within AMPbd and only a few within LID. Investigation of the results of MF and SRLS fitting indicated that in many cases MF selects model 5 instead of model 8, casting missed R_{ex}, and underrated τ_f and S_f^2, into S^2. In many other cases MF selects model 5 instead of model 6, casting underrated τ_f and S_f^2 into S^2. This constitutes force fitting[10] where minima abiding by statistical criteria, but featuring non-physical microdynamic parameters, are reached. Numerical simulations, where we generated synthetic model 6 and 8 data using SRLS and fitted those with MF, confirmed the observations outlined above. We also examined the effect of protein size (τ_m) and magnetic field value, to find that the MF digressions are significantly larger at 18.8 *T* than at 14.10 *T* for $\tau_m = 15.1$ ns.

Low NOEs did lead to low S^2 values for several AMPbd residues, colored yellow in Figure 6(left). In all of these cases MF selected the same model as SRLS. The common scenario also applies to 11.7 *T* data of RNase H,[7] which is a medium-size protein. With single-field data the only ns model possible is model 5, where $R_{ex} = 0$, so co-existence of ns and μs-ms motions is a mute point. Under these

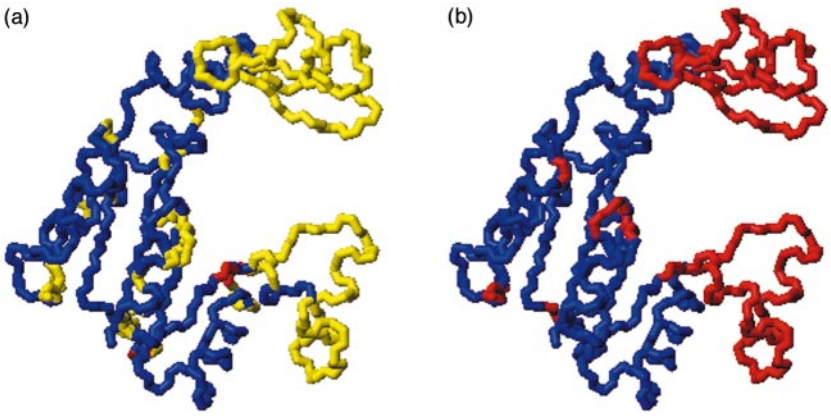

Figure 7. Ribbon diagrams of the crystal structure of AKeco color-coded according to MF τ_s values (a) and SRLS τ_s values (b). The Figure was drawn with the program Molscript[63] using the PDB coordinate file 4ake, and color-coded using the program MOLMOL[64]. Residues associated with isotropic local motion correlation time are colored blue. Residues with MF $\tau_s < 4$ ns are colored yellow. Residues pertaining to the ns SRLS regime are colored red. The color-coding is in accordance with Figure 4(c).

circumstances the tendency to force fitting is reduced significantly, and MF selects consistently the same model as SRLS.[7] Since literature reports are mostly similar to the RNase H rather than AKeco case, the common observation is that low NOEs correspond to low MF S^2 values. We conclude that the uncommon scenario is caused by force fitting promoted by the unusual co-existence within AMPbd and LID of ns local motions and segmental-mobility-related μs-ms conformational exchange. This is further enhanced by large MF inaccuracies featured by 18.79 *T* data generated by a relatively large protein. The S^2 profile becomes nearly flat, failing to reproduce (Figure 6(a)) the raw NOE profile (Figure 3(c)). On the other hand, MF τ_s and τ_f differ to a large enough extent to reproduce the raw NOE profile, as illustrated in Figure 7(a).

Conclusions

Backbone dynamics of the multi-domain enzyme adenylate kinase from *E. coli* was elucidated with coupled-mode SRLS ^{15}N relaxation. Domain CORE, which is structurally preserved during catalysis, features a conventional rigid structure with rapidly fluctuating N-H bond vectors. The domains AMPbd and LID, involved in catalysis-related domain motion, experience collective nanosecond peptide plane motions interpretable as domain motion. To our knowledge this is the first accurate experimental determination of domain motion correlation time. Coupled-mode SRLS ^{15}N relaxation is expected to be generally useful for studying domain motion in enzymes and other multiple-domain systems. It is expected to impact on studies of protein dynamics in general, and slow local motions in proteins, in particular. Cross-correlated relaxation studies,[44,45] and structure determination based on residual dipolar couplings,[46] may be extended to include local nanosecond dynamics if combined with SRLS.

Materials and Methods

NMR sample

For preparation of uniformly ^{15}N-labeled AKeco, *E. coli* HB101 cells transformed with pEAK91 plasmid were grown at 37 °C in Celtone-N medium (Martek Biosciences Corp., US) containing >98 % ^{15}N. The recombinant plasmid pEAK91 contained the intact gene coding for *E. coli* adenylate kinase.[47] The previously described procedure for purification of AKeco[22] was improved by application of Blue-Sepharose affinity chromatography,[47] followed by size-exclusion chromatography on a Sephacryl S-100 column (Pharmacia, Sweden). AKeco stock solution was prepared by thorough dialysis of the protein solution against 40 mM sodium-phosphate buffer (pH 6.8) containing 10 μM sodium azide, followed by concentration on a Centricon-10 concentrator (Amicon, US). The concentration of the AKeco solution was determined based on the absorption coefficient $A_{277} = 0.5$ mg/ml^{-1} cm^{-1}.[48] The sample was diluted to a final volume of 270 μl in 95%H_2O/5 %^2H_2O; it contained 1.75 mM solution of ^{15}N-labeled AKeco. The protein sample was degassed and transferred to a 5 mm NMR Shigemi cell. Protein mono-dispersion was ascertained previously.[23]

NMR spectroscopy

NMR experiments were carried out at 303 K on Bruker DMX-500, DMX-600 and DRX-800 spectrometers operating at 11.75, 14.10 and 18.79 *T*, respectively, using 5 mm ^{1}H-^{13}C-^{15}N triple resonance inverse detection probes and B-VT-2000 and BTO-2000 temperature control units at 14.10 and 18.79 T, respectively. NMR data were analyzed using the software packages NMRPipe and modelXY[49] on Silicon Graphics workstations. The previously determined assignments of the ^{1}H-^{15}N correlations,[50] complemented and revised in our earlier study,[23] were used.

Relaxation times T_1 and T_2, and NOE parameters were measured using established inversion recovery,[51] spin-echo,[52] and ^{15}N-{^{1}H} steady-state NOE[53] pulse sequences, as described.[54–56] A 1 ms delay between successive 180 ° ^{15}N pulses was used in the CPMG sequence. For $T_{1\rho}$ experiments we used the pulse sequences of references 55 and 57. For NOE experiments we used sequence 1B,[56] which features H_2O flip-back pulses to minimize saturation of water. Spectral widths were 1824.5 and 2432.6 Hz in the F_1 dimension and 9615.4 and 12820.5 Hz in the F_2 dimension at 14.10 and 18.79 *T*, respectively. The ^{15}N carrier was set at 117.5 ppm and was referenced indirectly to liquid NH_3.[58] 360×2048 complex points were acquired in the $t_1 \times t_2$ dimensions for each time point.

The ^{15}N T_1, T_2 and $T_{1\rho}$ measurements were performed using a total of 40, 64 and 64 transients per t_1 experiment, respectively. $T_{1\rho}$ was only measured at 14.10 *T*. For the T_1 measurements nine time points were collected, using parametric delays of 15, 127, 247, 367, 487, 647, 807, 1031 and 1287 ms at 14.10 *T*, and 15, 127, 327, 567, 807, 1047, 1367, 1767 and 2247 ms at 18.79 *T*. The experiment was repeated twice for time-points 15, 487 and 1287 ms at 14.10 *T*, and 15, 807 and 2247 ms at 18.79 *T*. The delay between scans was set to 1.5 seconds at 14.10 *T* and two seconds at 18.79 *T*. For the T_2 and $T_{1\rho}$ measurements nine time points were collected using parametric delays of 8, 16, 24, 32, 48, 64, 80, 96 and 128 ms at 14.10 *T*. For T_2 eight time points were collected using parametric delays of 8, 16, 32, 48, 64, 80, 104, 128 ms at 18.79 *T*. The experiment was repeated twice for time-points 8, 64, and 128 ms. The delay between scans was 1.6 s for T_2 and 2.5 s for $T_{1\rho}$ at 14.10 *T* and 1.9 s for T_2 at 18.79 *T*. The spin lock power used in the $T_{1\rho}$ experiments was 2.5 kHz. The data were apodized with a cosine-bell (squared cosine-bell) window function in t_1 (t_2). Duplicates were used to calculate average values of, and uncertainties in, the measured peak heights. Phenomenological T_1 and T_2 values and uncertainties were determined by non-linear least-squares fitting of the experimental data to monoexponential equations.[59]

The ^{15}N-{^{1}H} NOE values were measured using pairs of spectra recorded in an interleaved mode with and without proton presaturation during the recycle delay. A total of 96 transients per t_1 experiment were recorded. The delay between scans was six seconds at 11.75 *T*, 3.8

and 6.6 seconds at 14.10 *T* and 5.4 seconds at 18.79 *T*. Data were processed as described above. The ^{15}N-{^{1}H} NOE values were recorded in duplicate, and the replicates were used to determine uncertainties and mean values.

Data analysis

The calculation of SRLS spectral densities is computationally intensive for c_{20} values exceeding ~10 (S^2 exceeding ~0.81) and/or very fast internal motions. Therefore, in adapting SRLS to protein relaxation analysis we used pre-calculated two-dimensional grids of $j(0)$, $j(\omega_N)$, $j(\omega_H)$, $j(\omega_H + \omega_N)$ and $j(\omega_H - \omega_N)$ to fit experimental ^{15}N T_1, T_2 and ^{15}N-{^{1}H} NOE data.[7] The $j_{K=0}$, $j_{K=1}$ and $j_{K=2}$ grids of spectral density values at the five frequencies were constructed under the assumption of isotropic global motion for sets of c_{20} and τ_f (or τ_s) values. An axial ^{15}N chemical shielding tensor with $\sigma_\parallel - \sigma_\perp = -170$ ppm, $r_{NH} = 1.02$ Å and $\theta = -16^\circ$ (e.g. see ref. 60) were used in these calculations. The c_{20} grid dimension spanned the values between 0 ($S^2 = 0$) and 40 ($S^2 = 0.95$), and the τ dimension spanned the values between 0.0005 τ_m and 1.4τ_m. A two-dimensional polynomial interpolation using Neville's algorithm[61] was employed for spectral density evaluation in the course of model fitting. The interpolation errors in both the c_{20} and τ grid dimensions were estimated to be at least one order of magnitude smaller than the errors in fitted microdynamic parameters. The fitting of experimental NMR data† was based on Powell minimization[61] of a target function. The target function for spin i was defined as the sum of the squared differences between experimental and calculated T_1, T_2 and ^{15}N-{^{1}H} NOE values divided by the squared experimental errors:

$$\begin{aligned}\chi_i^2 = \Sigma[(T_{1i}^{obs} - T_{1i}^{calc})/\sigma_{T1,i}]^2 \\ + [(T_{2i}^{obs} - T_{2i}^{calc})/\sigma_{T2,i}]^2 \\ + [(NOE_i^{obs} - NOE_i^{calc})/\sigma_{NOEi}]^2\end{aligned} \quad (9)$$

where the sum runs over the magnetic fields used in acquiring the experimental data. The model selection scheme employed in the fitting program was based on χ^2 and F-statistic testing and closely followed that commonly used for MF analysis, as described.[7] Errors in microdynamic parameters were evaluated based on Monte-Carlo simulations[62] using 100 randomly distributed synthetic data sets.

The fundamentals of the MF calculations were described earlier.[32] A global diffusion correlation time of 15.1 ns was used in the MF analysis.[23] The program DYNAMICS[43] was used to determine the MF parameters, with the χ^2 probability confidence level set at 5%, and the *F*-statistic probability confidence level at 20%. The ^{15}N CSA value $\sigma_\parallel - \sigma_\perp = -170$ ppm and $r_{NH} = 1.02$ Å was used in all calculations.

† The pre-calculated $j_K(\omega)$ spectral density functions required for 2D grid generation, the data-fitting and model-selection program and associated files, the simulation program for calculating the experimental variables and documentation will be made available to the public shortly by the authors at an accessible web site.

Acknowledgments

This work was supported by the Israel Science Foundation grant number 520/99-16.1 (to E.M.), the Damadian Center for Magnetic Resonance Research at Bar-Ilan University, and an NIH NCRR grant to J.H.F. E.M. gratefully acknowledges the hospitality of CSIT, FSU, Tallahassee, FL, during short visits promoting this work; we also thank CSIT for computational resources. We thank Dr David Fushman (University of Maryland, College Park, MD) for sharing with us his program DYNAMICS.

References

1. Kay, L. E. (1998). Protein dynamics from NMR. *Nature Struct. Biol.* **5**, 513-517.
2. Ishima, R. & Torchia, D. A. (2000). Protein dynamics from NMR. *Nature Struct. Biol.* **7**, 740-743.
3. Peng, J. W. & Wagner, G. (1994). Investigation of protein motions *via* relaxation measurements. In *Methods in Enzymology* (James, T. L. & Oppenheimer, N. J., eds), vol. 239, pp. 563-595, Academic Press, New York.
4. Lipari, G. & Szabo, A. (1982). Model-free approach to the interpretation of NMR relaxation in macromolecules. 1. Theory and range of validity. *J. Am. Chem. Soc.* **104**, 4546-4559.
5. Lipari, G. & Szabo, A. (1982). Model-free approach to the interpretation of NMR relaxation in macromolecules. 2. Analysis of experimental results. *J. Am. Chem. Soc.* **104**, 4559-4570.
6. Clore, G. M., Szabo, A., Bax, A., Kay, L. E., Driscoll, P. C. & Gronenborn, A. M. (1990). Deviations from the simple two-parameter model-free approach to the interpretation of ^{15}N nuclear magnetic relaxation of proteins. *J. Am. Chem. Soc.* **112**, 4989-4991.
7. Tugarinov, V., Liang, Z., Shapiro, Yu. E., Freed, J. H. & Meirovitch, E. (2001). A structural mode-coupling approach to ^{15}N NMR relaxation in proteins. *J. Am. Chem. Soc.* **123**, 3055-3063.
8. Polimeno, A. & Freed, J. H. (1993). A many-body stochastic approach to rotational motions in liquids. *Advan. Phys. Chem.* **83**, 89-210.
9. Polimeno, A. & Freed, J. H. (1995). Slow motional ESR in complex fluids: the slowly relaxing local structure model of solvent cage effects. *J. Phys. Chem.* **99**, 10995-11006.
10. Liang, Z. & Freed, J. H. (1999). An assessment of the applicability of multifrequency ESR to study the complex dynamics of biomolecules. *J. Phys. Chem. ser. B*, **103**, 6384-6396.
11. Barnes, J. P., Liang, Z., Mchaourab, H. S., Freed, J. H. & Hubbell, W. L. (1999). A multifrequency electron spin resonance study of T4 lysozyme dynamics. *Biophys. J.* **76**, 3298-3306.
12. Liang, Z., Freed, J. H., Keyes, R. & Bobst, A. M. (2000). An electron spin resonance Study of DNA dynamics using the slowly relaxing local structure model. *J. Phys. Chem. ser. B*, **104**, 5372-5381.
13. Bennett, W. S. & Huber, R. (1984). Structural and functional aspects of domain motions in proteins. *Crit. Rev. Biochem.* **15**, 291-384.
14. Noda, L. (1973). Adenylate kinase. In *The Enzymes* (Boyer, P. D., ed.), vol. 8, pp. 279-305, Academic Press, New York.

15. Müller, C. W., Schlauderer, G. J., Reinstein, J. & Schulz, G. (1996). Adenylate kinase motions during catalysis: an energetic counterweight balancing substrate binding. *Structure,* **4**, 147-156.
16. Gerstein, M., Lesk, A. M. & Chothia, C. (1994). Structural mechanisms for domain movements in proteins. *Biochemistry,* **33**, 6739-6749.
17. Vornhein, C., Schlauderer, G. J. & Schulz, G. (1995). Movie of the structural changes during a catalytic cycle of nucleoside monophosphate kinases. *Structure,* **3**, 483-490.
18. Müller-Dickermann, H.-J. & Schulz, G. E. (1995). Substrate-specificity and assembly of catalytic center derived from two structures of ligated uridylate kinase. *J. Mol. Biol.* **246**, 522-530.
19. Müller, C. W. & Schulz, G. (1992). Structure of the complex between adenylate kinase from *Escherichia coli* and the inhibitor AP_5A refined at 1.9 Å resolution - a model for a catalytic transition state. *J. Mol. Biol.* **224**, 159-177.
20. Berry, M. B., Meador, B., Bilderback, T., Liang, P. & Glaser, M. (1994). The closed conformation of a highly flexible protein-the structure of *Escherichia coli* adenylate kinase with bound AMP and AMPPNP. *Proteins: Struct. Funct. Genet.* **19**, 183-198.
21. Sinev, M. A., Sineva, E. V., Ittah, V. & Haas, E. (1996a). Domain closure in adenylate kinase. *Biochemistry,* **35**, 6425-6437.
22. Sinev, M. A., Sineva, E. V., Ittah, V. & Haas, E. (1996b). Towards a mechanism of AMP-substrate inhibition in adenylate kinase from *Escherichia coli*. *FEBS Letters,* **397**, 273-276.
23. Shapiro, Y. E., Sinev, M. A., Sineva, E. V., Tugarinov, V. & Meirovitch, E. (2000). Backbone dynamics of *Escherichia coli* adenylate kinase at the extreme stages of the catalytic cycle studied by ^{15}N NMR relaxation. *Biochemistry,* **39**, 6634-6664.
24. Freed, J. H. (1976). *Spin Labeling: Theory and Applications* (Berliner, L. J., ed.), p. 53, Academic Press, New York.
25. Freed, H. J., Nayeem, A. & Rananavare, S. B. (1994). *The Molecular Dynamics of Liquid Crystals* (Luckhurst, G. R. & Veracini, C. A., eds), chapt. 12, pp. 271-312, Kluwer Academic Publishers, The Netherlands.
26. Freed, J. H. (1977). Stochastic-molecular theory of spin relaxation for liquid crystals. *J. Chem. Phys.* **66**, 4183-4199.
27. Fushman, D. & Cowburn, D. (1999). The effect of noncollinearity of ^{15}N-^{1}H dipolar and ^{15}N CSA tensors and rotational anisotropy on ^{15}N relaxation. CSA/dipolar cross-correlation and TROSY. *J. Biomol. NMR,* **13**, 139-147.
28. Abragam, A. (1961). *Principles of Nuclear Magnetism*, Oxford University Press (Clarendon), London.
29. Lin, W.-J. & Freed, J. H. (1979). The DRLS (equation B6). Electron spin resonance studies of anisotropic ordering, spin relaxation, and slow tumbling in liquid crystalline solvents. 3 Smectics. *J. Phys. Chem.* **83**, 379-401.
30. Kay, L. E., Torchia, D. A. & Bax, A. (1989). Backbone dynamics of proteins as studied by ^{15}N inverse detected heteronuclear NMR spectroscopy. Application to staphylococcal nuclease. *Biochemistry,* **28**, 8972-8979.
31. Lee, L. K., Rance, M., Chazin, W. J. & Palmer, A. G., III (1997). Rotational diffusion anisotropy of proteins from simultaneous analysis of ^{15}N and $^{13}C^{\alpha}$ nuclear spin relaxation. *J. Biomol. NMR,* **9**, 287-298.
32. Mandel, A. M., Akke, M. & Palmer, A. G., III (1995). Backbone dynamics of *Escherichia coli* ribunuclease HI: correlations with structure and function in an active enzyme. *J. Mol. Biol.* **246**, 144-163.
33. Lienin, S. F., Bremi, T., Brutcher, B., Brüschweiler, R. & Ernst, R. R. (1998). Anisotropic intramolecular backbone dynamics of ubiquitin characterized by NMR relaxation and MD computer simulation. *J. Am. Chem. Soc.* **129**, 9870-9879.
34. Schulz, G. E. & Schirmer, R. H. (1990). *Principles of Protein Structure* (Cantor, C. R., ed.), p. 18, Spinger-Verlag, New York.
35. Polnaszek, C. F. & Freed, J. H. (1975). Electron spin resonance studies of anisotropic ordering, spin relaxation, and slow tumbling in liquid crystalline solvents. 1. *J. Phys. Chem.* **79**, 2283-2306.
36. Lienin, S. F. & Brüschweiler., R. (2000). Characterization of collective and anisotropic reorientational protein dynamics. *Phys. Rev. Letters,* **84**, 5439-5442.
37. Prompers, J. J. & Brüschweiler, R. (2000). Thermodynamic interpretation of NMR parameters in proteins in the presence of motional correlations. *J. Phys. Chem. ser. B,* **104**, 11416-11424.
38. Mason, R. P., Polnaszek, C. F. & Freed, J. H. (1974). Comment on the interpretation of electron spin resonance spectra of spin labels undergoing very anisotropic rotational reorientation. *J. Phys. Chem.* **78**, 1324-1329.
39. Millet, O., Loria, J. P., Kroenke, C. D., Pons, M. & Palmer, A. G., III (2000). The static magnetic field dependence of chemical exchange linebroadening defines the NMR chemical shift time scale. *J. Am. Chem. Soc.* **122**, 2867-2877.
40. Fushman, D. & Cowburn, D. (1998). Model-independent analysis of ^{15}N chemical shift Anisotropy from NMR relaxation data. Ubiquitin as a test example. *J. Am. Chem. Soc.* **120**, 7109-7110.
41. Tjandra, N., Szabo, A. & Bax, A. (1996). Protein backbone dynamics and ^{15}N chemical shift anisotropy from quantitative measurement of relaxation interference. *J. Am. Chem. Soc.* **118**, 6986-6991.
42. La Penna, G., Fausti, S., Perico, A. & Ferretti, J. A. (2000). Smoluchowski dynamics of the vnd/NK-2 homeodomain from *Drosophila melanogaster*: second-order maximum correlation approximation. *Biopolymers,* **54**, 89-103.
43. Fushman, D., Cahill, S. & Cowburn, D. (1997). The main-chain dynamics of the dynamin pleckstrin homology (PH) domain in solution: analysis of ^{15}N relaxation with monomer/dimer equilibration. *J. Mol. Biol.* **266**, 173-194.
44. Pellechia, M., Pang, Y., Liocong, W., Kurochin, A. V., Kumar, A. & Zuiderweg, E. R. P. (1999). Quantitative measurement of cross-correlations between ^{15}N and ^{13}CO chemical shift anisotropy relaxation mechanisms by multiple quantum NMR. *J. Am. Chem. Soc.* **121**, 9165-9170.
45. Pang, Y. & Zuiderweg, E. R. P. (2000). Determination of protein backbone ^{13}CO chemical shift anisotropy tensors in solution. *J. Am. Chem. Soc.* **122**, 4841-4842.
46. Cornilescu, G. & Bax, A. (2000). Measurement of proton, nitrogen, and carbonyl chemical shielding anisotropies in a protein dissolved in a dilute liquid crystalline phase. *J. Am. Chem. Soc.* **122**, 10143-10154.
47. Reinstein, J., Brunne, M. & Wittinghofer, A. (1988). Mutations in the nucleotide binding loop of *Escherichia coli* adenylate kinase. *Biochemistry,* **27**, 4712-4720.

48. Girons, I. S., Gilles, A.-M., Margarita, D., Michelson, S., Monnot, M., Fermandjian, S. *et al*. (1987). Structural and catalytic characteristics of *Escherichia coli* adenylate kinase. *J. Biol. Chem.* **262**, 622-629.
49. Delaglio, F., Grzesiek, S., Vuister, G. W., Zhu, G., Pfeifer, J. & Bax, A. (1995). NMRPipe - a multidimensional spectral processing system based on UNIX pipes. *J. Biomol. NMR*, **6**, 277-293.
50. Burlacu-Miron, S., Perrier, V., Gilles, A.-M., Mispelter, J., Barzu, O. & Craescu, C. T. (1999). ^{1}H, ^{13}C and ^{15}N backbone resonance assignment of *Escherichia coli* adenylate kinase, a 23.6 kDa protein. *J. Biomol. NMR,* **13**, 93-94.
51. Vold, R. L., Waugh, J. S., Klein, M. P. & Phelps, D. E. (1968). Measurement of spin-relaxation in complex system. *J. Chem. Phys.* **48**, 3831-3832.
52. Meiboom, S. & Gill, D. (1958). Modified spin-echo method for measuring nuclear spin relaxation rates. *Rev. Sci. Instrum.* **29**, 688-691.
53. Noggle, J. H. & Shirmer, R. E. (1971). *The Nuclear Overhauser Effect: Chemical Aplications*, Academic Press, New York.
54. Kay, L. E., Nicholson, L. K., Delaglio, F., Bax, A. & Torchia, D. A. (1992). Pulse sequences for removal of the effects of cross-correlation between dipolar and chemical shift anisotropy relaxation mechanisms on the measurement of heteronuclear T_1 and T_2 values in protein. *J. Magn. Res.* **97**, 359-375.
55. Palmer, A. G., III, Skelton, N. J., Chazin, W. J., Wright, P. E. & Rance, M. (1992). Suppression of the effects of cross-correlation between dipolar and chemical shift anisotropy relaxation mechanisms in the measurement of spin-spin relaxation rates. *Mol. Phys.* **75**, 699-711.
56. Grzesiek, S. & Bax, A. (1993). The importance of not saturating H_2O in protein NMR. Application to sensitivity enhancement and NOE measurement. *J. Am. Chem. Soc.* **115**, 12593-12594.
57. Szyperski, T., Lüginbuhl, P., Otting, G., Güntert, P. & Wüthrich, K. (1993). Protein dynamics studied by rotating frame ^{15}N spin relaxation rates. *J. Biomol. NMR,* **3**, 151-164.
58. Live, D. H., Davis, D. G., Agosta, W. C. & Cowburn, D. (1984). Long-range hydrogen bond mediated effects in peptides: ^{15}N NMR study of gramicidin S in water and organic solvents. *J. Am. Chem. Soc.* **106**, 1939-1941.
59. Palmer, A. G., III, Rance, M. & Wright, P. E. (1991). Intermolecular motions of zinc finger DNA-binding domain from Xfin characterized by proton-detected natural abundance ^{13}C heteronuclear NMR spectroscopy. *J. Am. Chem. Soc.* **113**, 4371-4380.
60. Fushman, D., Tjandra, N. & Cowburn, D. (1998). Direct measurement of ^{15}N chemical shift anisotropy in solution. *J. Am. Chem. Soc.* **120**, 10947-10952.
61. Press, W. H., Teukolsky, S. A., Vetterling, W. T. & Flannery, B. P. (1992). *Numerical Recipes in C. The Art of Scientific Computing*, Cambridge University Press, Cambridge.
62. Kamath, U. & Shriver, J. W. (1989). Characterization of thermotropic changes in myosin subfragment-1 and heavy-meromyosin by UV difference spectroscopy. *J. Biol. Chem.* **264**, 5586-5592.
63. Kraulis, P. J. (1991). Molscript: a program to produce both detailed and schematic plots of protein structures. *J. Applied Crystallog.* **24**, 946-995.
64. Koradi, R., Billeter, M. & Wüthrich, K. (1996). MOLMOL: a program for display and analysis of macromolecular structures. *J. Mol. Graph.* **14**, 51-55.

Edited by P. E. Wright

(Received 25 July 2001; received in revised form 2 November 2001; accepted 2 November 2001)

http://www.academicpress.com/jmb

Supplementary Material is available from IDEAL consisting of the following. ^{15}N T_1, T_2 and ^{15}N-{^{1}H} NOE data of *E. coli* adenylate kinase acquired at 14.10 and 18.79 *T* at 303K (Table S1, 5 pages). The results of SRLS fitting based on the combined data set, including estimated errors of the best-fit parameters (Table S2, 6 pages). The results of MF fitting based on the combined data set, including estimated errors of the best-fit parameters (Table S3, 4 pages).